iScience

CellPress
OPEN ACCESS

Article

Phase diagram simulations incorporating the gap anisotropy with AFM spin and charge density wave under spin-orbital coupling in Fe-based superconductors

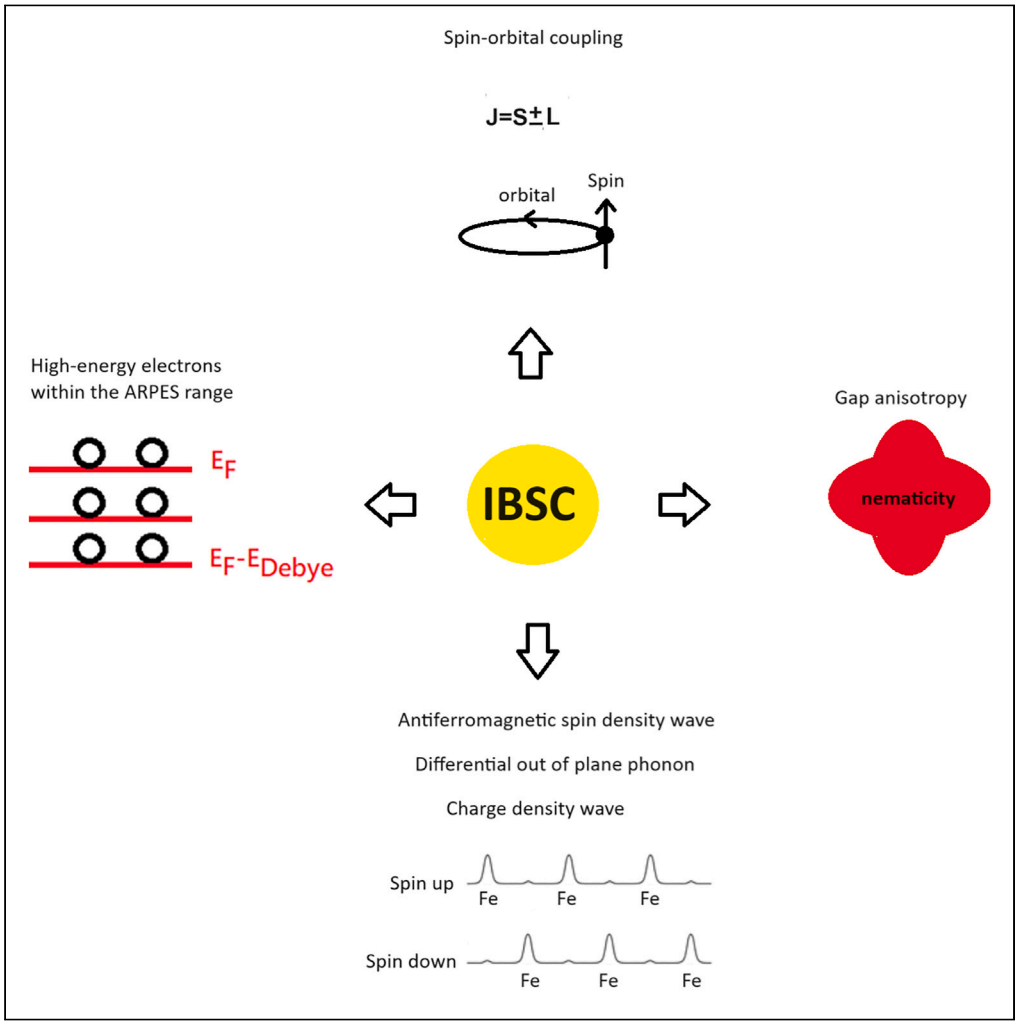

Chi Ho Wong, Rolf Lortz

chkhwong@ust.hk (C.H.W.)
lortz@ust.hk (R.L.)

Highlights

First-ever T_c formula for calculating the T_c of major IBSCs as a function of pressure

The roles of first and higher-order AFM fluctuation in the T_c values are identified

The effect of the high-energy electrons on the T_c values is observed

Sample quality plays a role to affect the T_c of FeSe/STO

Wong & Lortz, iScience 27, 110204
July 19, 2024
https://doi.org/10.1016/j.isci.2024.110204

iScience

CellPress
OPEN ACCESS

Article

Phase diagram simulations incorporating the gap anisotropy with AFM spin and charge density wave under spin-orbital coupling in Fe-based superconductors

Chi Ho Wong[1,2,3,*] and Rolf Lortz[1,*]

SUMMARY

For over a decade, iron-based superconductors (IBSCs) have been the subject of intense scientific research, yet the underlying principle of their pairing mechanism remains elusive. To address this, we have developed a simulation tool that reasonably predicts the regional superconducting phase diagrams of key IBSCs, incorporating factors such as anisotropic superconducting gap, spin-orbital coupling, electron-phonon coupling, antiferromagnetism, spin density wave, and charge transfer. Our focus has been on bulk FeSe, LiFeAs, NaFeAs, and FeSe films on $SrTiO_3$ substrates. By incorporating angle-resolved photoemission spectroscopy (ARPES) data to fine-tune the electron concentration in the superconducting state, our simulations have successfully predicted the theoretical superconducting transition temperature (T_c) of these compounds, closely matching experimental results. Our research not only aids in identifying patterns and establishing correlations with T_c but also provides a simulation tool for potentially predicting high-pressure phase diagrams.

INTRODUCTION

The pairing mechanism of unconventional high-temperature superconductors (HTSCs) remains a significant enigma in the realm of physics. Iron-based superconductors (IBSCs) consistently exhibit five shared characteristics.[1,2] These include a momentum-dependent superconducting gap, spin-orbital coupling, antiferromagnetic fluctuations, nematic order, and a spin density wave (SDW).[1–4] A multitude of theoretical approaches underscore the importance of spin fluctuations in unconventional superconductors.[5,6] Consequently, the development of a comprehensive theoretical model that leverages spin fluctuations to predict the complete superconducting phase diagram under varying pressure conditions seems to be a logical and promising direction.

Antiferromagnetiic (AFM) effect enhances electron-phonon coupling in IBSC,[7–10] while the combination of AFM and SDW in IBSC leads to a constructive-like interference effect, further amplifying local AFM fluctuations. Out-of-plane phonon is then contributed to electron-phonon coupling, with the imbalanced out-of-plane displacement of Fe atoms facilitating a local electric potential across the magnetic and non-magnetic boundaries under SDW, where atomic vibrations in the magnetic regions are usually slower. The significant AFM fluctuations under the constructive-like interference suggest that the mean-field density functional theory (DFT) approach may not accurately describe IBSCs. Hence, the impact of differential out-of-plane phonons in IBSC should be included in the superconducting transition temperature (T_c) calculations. On the other hand, nanostructuring could be a way to improve the Tc of IBSC such as FeSe monolayers on $SrTiO_3$ substrates achieving Tc values of 100 K.[10–13] High-energy phonons, particularly Fuchs-Kliewer F-K phonons (1,159 K),[13–18] are implicated in the unconventional pairing mechanism of IBSC, as observed in the FeSe/$SrTiO_3$ interface. However, the reason for variations in T_c of FeSe/$SrTiO_3$, ranging from 20 to 80 K, remains an open question.

In the study of unconventional superconductors, it is commonly believed that the Cooper pairing mechanism cannot be explained solely by a standard scenario involving electron-phonon coupling on the Fermi surface. However, it is possible that considering this interaction on the Fermi surface alone might be insufficient to account for all the relevant electrons involved in HTSCs, because angle-resolved photoemission spectroscopy (ARPES) data actually demonstrate that the onset of superconductivity influences the distribution of electrons as far as ~0.03–0.3 eV below the Fermi energy E_F in IBSC (abbreviated in the following as "ARPES range").[17–19] To conduct an in-depth analysis of the formation of Cooper pairs in IBSC, we have taken into account the actual concentration of superconducting electrons while considering the five common characteristics in HTSCs together.

[1]Department of Physics, The Hong Kong University of Science and Technology, Hong Kong, China
[2]Department of Industrial and Systems Engineering, The Hong Kong Polytechnic University, Hong Kong, China
[3]Lead contact
*Correspondence: chkhwong@ust.hk (C.H.W.), lortz@ust.hk (R.L.)
https://doi.org/10.1016/j.isci.2024.110204

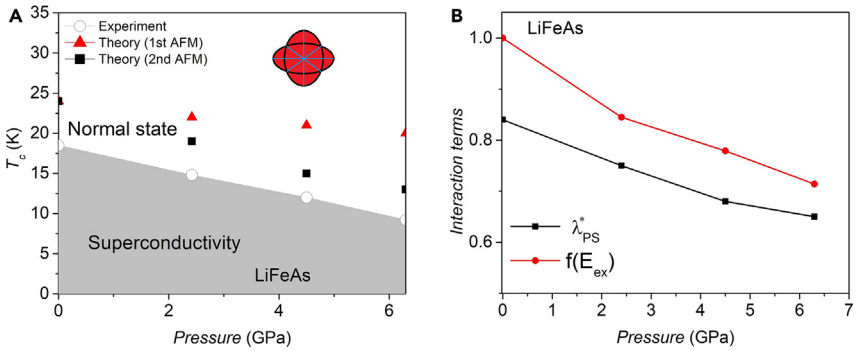

Figure 1. The theoretical and experimental T_c values of LiFeAs are found to be close with each other when the pressure dependence of pairing strength is monitored by 2nd AFM fluctuation

(A) The T_c vs. pressure of LiFeAs. The 4-fold symmetry in the k space of LiFeAs[20–22] can be visualized by two overlapped red ellipses. The overlap region is divided into 8 equal partitions using blue lines, resulting in 8 distinct regions. Each of these regions has an equal area, denoted as $\int_0^{\pi/4} \frac{1}{2} \rho_{angular}(\theta)^2 d\theta$.

(B) The pairing strength and the antiferromagnetic exchange factor under pressure are plotted. These factors play a crucial role in understanding the behavior of LiFeAs superconductor and its response to changes in pressure.

It is important to clarify that the objective of this paper is not to put forth a theory of IBSCs. Instead, our focus is on the development of a specialized simulation tool tailored for the simulation of phase diagrams of IBSC, particularly under the influence of pressure. This tool can be employed once a sample has confirmed the existence of IBSC at ambient pressure. Furthermore, it provides the opportunity to investigate the complex interplay between electron-phonon interaction, superconductivity, and magnetic properties, which may also hint at the origin of the T_c offset in FeSe/$SrTiO_3$.

RESULTS

In Figure 1A, the phase-diagram simulation of LiFeAs superconductor is presented. It reveals that the 1st-order antiferromagnetic (AFM) fluctuation exhibits a significant error in the pressure dependence on the T_c compared to the 2nd-order AFM fluctuation. Figure 1B showcases the pairing strength under the 2nd-order AFM fluctuation and the exchange factor. Interestingly, both parameters show a decrease under pressure, which perplexes the observed reduction in T_c under pressure. When the pressure is increased from 0 to 6 GPa, R_{ARPES} exhibits a slight increase from 2.6 to 2.8. The effect of charge transfer in the tetrahedral region shows a computed value of $R_{ph}|_{P=0} = 1.34$. Furthermore, we have also used the literature results[7,8] for our analysis in which $R^2_{AFM}|_{P=0} = 1.68$ and $R_{SDW} = 2$. Another literature study on LiFeAs has revealed that the momentum dependence on the superconducting gap can exhibit a 4-fold symmetry.[20] This means that the magnitude of the superconducting gap varies with different directions in momentum space. Upon considering the shape of the anisotropic wave vector in k-space, the pairing strength decreases by 42% due to $f_{anisotropy}$. This finding also suggests that the presence of anisotropy leads to a decrease in the average pairing strength compared to the isotropic case.[21] As an example, we show the T_c calculation of LiFeAs at 0 GPa in the supplemental information.

The ARPES data for NaFeAs show neither an unusual distribution of electrons below the Fermi level nor momentum dependence on the superconducting gap. Hence, we set $R_{ARPES} = 1$ and $f_{anisotropy} = 1$. Meanwhile, our two-channel model gives $R_{ph}|_{P=0} = 1.51$. By using the literature result, we obtain $R^2_{AFM} = 1.62$ for NaFeAs at 0 GPa.[7] Figure 2 shows the calculated T_c of NaFeAs as a function of pressure after incorporating the parameters into AFM fluctuation. To calculate the T_c of uncompressed NaFeAs, we have listed the steps mentioned in the supplemental information.

Under compression, the behavior of FeSe exhibits enhanced AFM fluctuations, resulting in an increase in the T_c. This phenomenon is illustrated in Figure 3. Our approach utilizes a mean field methodology, which considers spin fluctuations to be proportional to the mean field Hamiltonian. As pressure increases, the optimized pairing strength in FeSe also increases. The ARPES factor in FeSe demonstrates an upward trend from 1.8 to ~3.5 at higher pressures, while we directly utilize a Coh factor of $R_{ph}R_{SDW}$=4.[8] When using spin-unrestricted mode rather than spin-restricted mode, the electron-phonon coupling is amplified by a factor of only 1.5. The gap equation is obtained from the literature,[24] which interprets that the anisotropy causes a ~40% decrease in the pairing strength based on the 4-fold symmetry. We calculate the T_c of an uncompressed FeSe superconductor in the supplemental information.

Our computational model enables us to calculate the highest T_c observed in the IBSC family, i.e., a FeSe monolayer on a $SrTiO_3$ substrate. Upon geometric optimization, we observed a change in the tetrahedral angle of Fe-Se-Fe from 104° to 108°, and a tiny lattice distortion is detected in the unit cell. It has been found that when FeSe is deposited as a monolayer on $SrTiO_3$, its antiferromagnetic energy can be enhanced due to low dimensionality.[13] The FeSe film on $SrTiO_3$ exhibits a 14% increase in exchange-correlation energy compared to bulk FeSe. In addition, the local magnetic moment of FeSe under the influence of the substrate increases from 0.5 to 1.2 μB in the role of internal pressure, which leads to a 6-fold increase in AFM fluctuation. The R_{ph} value, which represents the induced xy potential in the tetrahedral region, also increases from 2.1 to 2.9. even without multiplying by $f(E_{ex})$. Furthermore, the analysis of ARPES data reveals a notable shift in spectral weight within the superconducting state, approximately 0.1–0.3 eV below the Fermi level.[18] This shift suggests that electrons within this

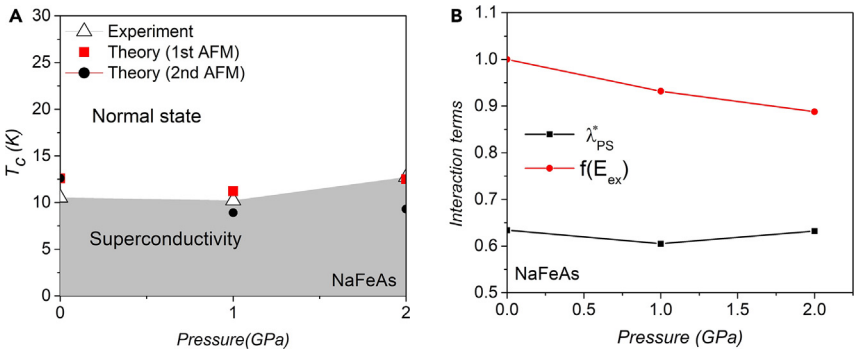

Figure 2. The theoretical and experimental T_c of NaFeAs vs. pressure

(A) The T_c values of NaFeAs, both theoretical and experimental,[23] are presented.

(B) The plots illustrate the relative changes in AFM fluctuation and the pairing strength under 1st AFM fluctuation, with pressure as the independent variable.

energy range undergo superconductivity. The Fuchs-Kliewer F-K phonon, activated through the interface, contributes a vibrational energy of approximately 100 meV (1,159 K).[16] The pairing strength is significantly enhanced when the interfacial F-K phonon is involved. This substantial vibrational energy, coupled with a high Debye temperature, results in a theoretical T_c value of 98 K. Remarkably, this calculated T_c closely aligns with the experimental T_c of 100 K.[18] Taken together, we should not overlook the role of interfacial phonons under antiferromagnetic SDWs in driving the superconducting behavior of the system. We demonstrate the T_c calculation of FeSe/$SrTiO_3$ in the supplemental information. However, lattice mismatch is a crucial factor influencing the stability of T_c values in FeSe/$SrTiO_3$ systems. Even a relatively small compressive surface strain of approximately 2.5% can significantly reduce the T_c value to around 20 K (see supplemental information).

DISCUSSION

When a material exhibits superconductivity at ambient pressure, it becomes intriguing to explore how the T_c may be influenced by applying pressure. Conducting experiments to directly measure T_c at high pressures, even at magnitudes of ~10–20 GPa, is a complex task.[26,27] Therefore, it becomes crucial to develop a superconducting phase-diagram simulator to predict T_c values under the influence of high pressure. Our development of the phase-diagram simulator incorporates momentum-dependent superconductivity using charge transfer in the tetrahedral regions in the presence of an antiferromagnetic SDW under spin-orbital coupling, which exhibits reasonably good accuracy in Figures 1, 2, and 3.

The T_c calculation in Figure 1A indicates that the pairing strength of LiFeAs is better suited for fitting second-order AFM fluctuations. This remark is drawn from observing that the error in T_c is much more serious when pressure is raised under the 1st-order AFM fluctuations. Figure 1B provides evidence that the decrease in T_c in LiFeAs can primarily be attributed to the suppression of AFM fluctuations at high pressures. On the other hand, in NaFeAs, a compensation effect is observed between 1 and 2 GPa, where there is an increase in pairing strength and a decrease in antiferromagnetic (AFM) fluctuation. As a result, there is no significant change in the T_c between 0 and 2 GPa in NaFeAs when compared to the situation in LiFeAs. In compressed FeSe, the magnetic moment of Fe increases, leading to an increase in AFM energy under pressure, and presumably, we observe an increase in the T_c. It is worth noting that at low pressure, there may not be a significant difference in the pairing strength when considering the effects of both 1st AFM and 2nd AFM fluctuations. This is because when the independent variable is small, it is possible for a dependence variable to be fitted linearly.

The ARPES factor slightly increases with pressure. This can be attributed to the higher Debye temperature, which allows for the averaging of more high-energy electrons to participate in the electron-phonon scattering. However, when pressure (or Debye energy) becomes too high, the ARPES factor may drop because of the accumulation of a large number of high-energy electrons, which intensifies the screening effect. The proportionality between the ARPES energy range and Debye energy is supported by comparing the ARPES data of the 100 K 2D FeSe/$SrTiO_3$[18] with other bulk IBSCs. In the case of these ~10–30 K bulk IBSCs, the electrons influenced by superconductivity are located at an energy range of 0.03–0.06 eV below the Fermi level.[17] However, in the 100 K 2D FeSe/$SrTiO_3$, the affected electrons span a wider range of 0.1–0.3 eV below the Fermi level,[18] and meanwhile the interfacial phonon shows an energy of 1,159 K (or 0.1 meV),[16] providing support for the 3- to 4-fold increase in proportionality. However, the Debye energy can be either lower or higher than the ARPES energy range that may introduce errors in the T_c calculations. In the FeSe/$SrTiO_3$ system, the R_{ph} value is observed to be 1.5 times higher compared to bulk FeSe. This difference in R_{ph} can be attributed to the structural asymmetry between the upper and lower tetrahedral regions within the FeSe layer. In this composite, the upper tetrahedral region exists in a vacuum space, while the lower tetrahedral region interacts with the $SrTiO_3$ substrate. The presence of the substrate leads to a reinforcement of the non-cancellable out-of-plane phonon,[8] which in turn strengthens the effect of the induced xy potential. The stability of experimental T_c values in FeSe/$SrTiO_3$ systems can be heavily influenced by lattice mismatch. A tiny compressive surface strain of around 2% can lead to a significant decrease in the T_c value, lowering it to approximately 20 K. This reduction in T_c can be primarily attributed to a substantial drop in the magnetic moment of the Fe atom, which decreases by almost one-fourth for strains up to approximately 2.5%. This proves its high T_c phenomenon is mainly driven by spin-spin fluctuation. According to our model, no calculated T_c value can exceed 99 K in FeSe/$SrTiO_3$. This can be easily verified by setting the absolute pairing strength to infinite.

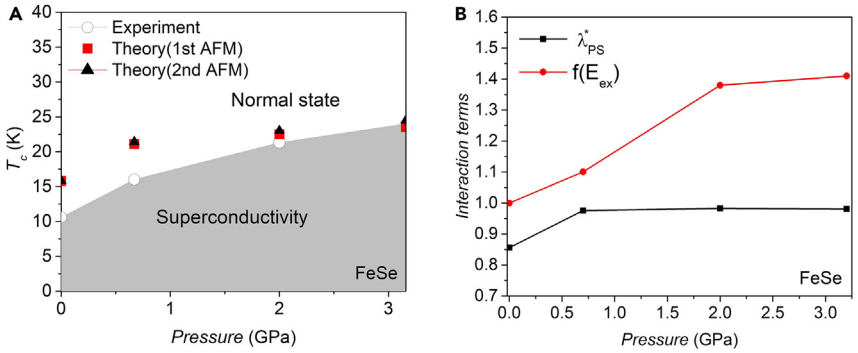

Figure 3. The theoretical and experimental T_c of bulk FeSe

(A) Both the theoretical and experimental[25] T_c values show an increase under pressure for FeSe.

(B) The pressure dependence of the pairing strength in the presence of 2nd AFM fluctuation is demonstrated.

Although the impact of spin-orbital coupling on electron-phonon coupling in these compounds may only be a few percent, it should not be underestimated or disregarded in understanding the pairing mechanism of IBSC. In the case of LiFeAs, for example, it has been experimentally confirmed that spin-orbit coupling (SOC) exists[28] where the presence of SOC affects the Fermi surface, specifically resulting in the disappearance of one of the 3D small-hole pockets near the Z point.[29] In the case of FeSe, the splitting of the bands increases more significantly away from the Γ point compared to the case without spin-orbit interaction (SOI).[30] This observation suggests that the effectiveness of Cooper pair formation under SOI is more dependent on the angular distribution within the momentum space. In summary, for both LiFeAs and FeSe, the presence of SOI leads to a more complex Fermi surface, and the effectiveness of triggering Cooper pair formation varies as a function of the angular momentum space. Our findings indicate that SOC only leads to minor changes, on the order of a few percent, in the absolute pairing strength when comparing systems with and without SOC. This is because the integration of momentum space, when considering systems with and without SOC, yields nearly identical numerical number. Then the absolute pairing strength with and without SOC remains almost the same after renormalization. Although our model is capable of predicting their T_c under compression, our work may not provide a comprehensive explanation of how electrons are paired in the complex environment of IBSC. In other words, spin-orbital coupling may play a key role in initiating electron pairing,[28] but once Cooper pairs are formed at 0 GPa, the influence of spin-orbital coupling on the stability of these pairs under pressure may become less pronounced. Nematicity also has the potential to influence the momentum dependence of the superconducting gap.[31] However, the exact relationship or formula connecting the gap anisotropy and nematicity remains unknown since 2008. In spite of this, we captured the experimental data[20,24] such as the anisotropic Fermi surface or the gap equation directly, to mimic the effect of nematicity preliminarily. It is worth noting that nematicity sometimes pales the connection between pairing strength and AFM fluctuation.[31] Even if nematicity pales the connection between them, the reduction in pairing strength by 50% as a result of gap anisotropy is not anticipated. Such a significant decrease in pairing strength could potentially lead to the emergence of a p-wave superconductor[32] which is not expected in these three samples. Fortunately, setting $0.5 < f_{anisotropy} < 1$ does not lead to a significant deviation in the calculated T_c. This argument is supported by our analysis of LiFeAs and FeSe. For instance, at 0 GPa, the error in the theoretical T_c of LiFeAs is only ± 2 K when we tune $0.5 < f_{anisotropy} < 1$, while for uncompressed FeSe it is only ± 1.5 K. This behavior is distinct from low-T_c BCS superconductors where renormalization would result in a larger change in T_c. The reason for this difference lies in the initial pairing strength of the materials before renormalization. In the case of LiFeAs and FeSe, the initial pairing strength is already very large, which means that even after renormalization, the resulting value remains very close to 1.

The interplay between different bands and their respective Fermi surfaces introduces additional degrees of freedom for spin excitations. Interband interactions between the Fermi surfaces may enhance spin fluctuations by promoting spin excitations between different bands, and hence it may raise the exchange factor to increase the T_c. However, the exchange factor is computed within the context of an all-in-one DFT calculation, ensuring that the interband interactions should be incorporated already. Although different DFT functionals handle the interband interactions in different ways, we utilize a range of DFT functional, such as BYLP, RPBE, PW91, PBESOL, m-GGA, and others, to estimate the exchange-correlation energy. The variation in the exchange-correlation energy among these different DFT functionals is typically below 2%. Even when considering higher-order exchange couplings, the resulting impact on the T_c is typically less than approximately 10%. This is because the difference between renormalizing two distinct large absolute pairing strengths is not readily apparent.

Our model does not exclusively rely on a phonon-driven mechanism (phonon is only a medium to collect the amplification effects of spin fluctuation); it incorporates spin fluctuations as a significant contributor to the pairing interaction. This approach bridges the gap with the traditional phonon-mediated scenario, wherein spin fluctuations markedly enhance the electron-phonon coupling. Our objective is to illustrate that this expanded framework, which we term as a spin-fluctuation-assisted and phonon-mediated scenario, could serve as a viable model for elucidating the phenomena observed in iron-based superconductivity. Our simulations demonstrate that, despite the application of a two-channel model, the phonon frequency undergoes only a minimal change, amounting to less than a few percent. However, the

two-channel model allows us to observe a clear increase in the electronic density of states and the local magnetic moment of Fe when the differential out-of-plane phonon emerges. Therefore, our findings suggest that the high T_c observed in this system is primarily driven by spin fluctuations, rather than phonon energy. However, in order to visualize and understand these phenomena more comprehensively, it is essential to analyze the effects of individual out-of-plane phonons on the electronic density of states (DOSs), instead of solely focusing on the impact of an average out-of-plane phonon on the DOS. It is important to note that phonon may act as a medium for collecting the robust effects arising from electron-electron interactions and spin fluctuations.

It is indeed possible to enhance the accuracy of our T_c simulator by incorporating additional factors. One approach is to separate the phonon data into acoustic and optical modes in the McMillian T_c formula selectively, allowing us to analyze the distinct phonon effects contributed by each mode. Such insights will be valuable for refining our T_c simulator and improving its accuracy in predicting T_c for different materials or scenarios. On the other hand, if the charge density wave (CDW) is dynamic and interacts with spin fluctuations, predicting the influence of these factors on superconducting pairing presents a significant challenge due to the intricate interplay of these phenomena. However, in our T_c simulator, we incorporate a methodology[33] to multiply the exchange enhancement factor with the pairing strength using a separation of variables. This may allow us to emulate the dynamic interaction between the CDW and spin fluctuations within the system at a small-pressure regime approximately. We have observed a notable rise in the electronic DOS at the interface between non-magnetic and magnetic regions within a SDW pattern. This substantial increase in the local electronic DOS at the interface suggests the presence of a CDW.

When compared to our old IBSC model,[34] our current IBSC model has significantly upgraded. The old IBSC model[34] was a preliminary version that represented our best effort available at that time. However, the model has been undergoing development and gaining insights over time. There were five limitations in the old IBSC model[34]: (1) it did not take into account the electrostatic screening effect when revising the electron concentration within the ARPES range; (2) it did not optimize the combined effects of antiferromagnetic fluctuation and SDW; (3) it also assumed s-wave pairing without conducting a thorough analysis of the momentum dependence of the superconducting gap that could arise from nematicity; (4) the effects of spin-orbital coupling and higher-order spin fluctuations were not considered either; and (5) it involved a multiplication of the exchange factor by the renormalized pairing strength empirically where the exchange factor should have been multiplied by the original pairing strength before renormalization. In contrast, here, our current IBSC model has addressed these 5 limitations.

Our simulator has proven to be effective in bridging the gap between theoretical and experimental T_c values in IBSC. Despite this, the pursuit of a comprehensive theory in this domain is still in progress, indicating the need for additional research and exploration. Our model offers a credible approach to explain the high T_c values observed in IBSC. This approach could potentially be applied to other unconventional superconductors in the future. However, it is important to note that there may be alternative models capable of accurately predicting the theoretical T_c of IBSC through entirely different mechanisms.

Limitations of the study

The current model demonstrates proficiency in handling various types of CDWs, including the major 11, 111, and 122 types. However, it should be noted that we look forward to encountering challenges when dealing with more complex CDW structures, such as the 1111-type. The mathematical formulation and analysis of such intricate CDW patterns may require further modifications and advancements. It is important to acknowledge that addressing these complexities is an ongoing area of research, and future improvements in modeling techniques may enhance our ability to effectively handle and interpret the intricacies of CDWs.

STAR★METHODS

Detailed methods are provided in the online version of this paper and include the following:

- KEY RESOURCES TABLE
- RESOURCE AVAILABILITY
  - Lead contact
  - Materials availability
  - Data and code availability
- EXPERIMENTAL MODEL AND STUDY PARTICIPANT DETAILS
- METHOD DETAILS
  - Charge transfer in the tetrahedral regions in the presence of AFM-SDW
  - ARPES analysis
  - Anisotropic k space
  - AFM & SDW amplified electron-phonon interaction under spin-orbital coupling
- QUANTIFICATION AND STATISTICAL ANALYSIS

SUPPLEMENTAL INFORMATION

Supplemental information can be found online at https://doi.org/10.1016/j.isci.2024.110204.

ACKNOWLEDGMENTS

We appreciate the Department of Industrial and Systems Engineering in the Hong Kong Polytechnic University to provide simulation facilitates.

AUTHOR CONTRIBUTIONS

Conceptualization, C.H.W. and R.L.; methodology, C.H.W.; software, C.H.W.; validation, C.H.W. and R.L.; formal analysis, C.H.W.; investigation, C.H.W.; resources, R.L.; data curation, C.H.W.; writing – original draft, C.H.W.; writing – review and editing, C.H.W. and R.L.; visualization, C.H.W.; supervision, C.H.W. and R.L.

DECLARATION OF INTERESTS

The authors declare no competing interests.

Received: March 8, 2024
Revised: April 7, 2024
Accepted: June 4, 2024
Published: June 6, 2024

SUPPORTING CITATIONS

The following references appear in the Supplemental Information: 37–39.

REFERENCES

1. Norman, M. (2008). High-temperature superconductivity in the iron pnictides. Physics *1*, 21.
2. Bednorz, J.G., and Müller, K.A. (1986). Possible high Tc superconductivity in the Ba−La−Cu−O system. Z. Phys. B *64*, 189–193.
3. Fernandes, R.M., Chubukov, A.V., and Schmalian, J. (2014). What drives nematic order in iron-based superconductors? Nat. Phys. *10*, 97–104.
4. Grüner, G. (1988). The dynamics of charge-density waves. Rev. Mod. Phys. *60*, 1129–1181.
5. V.L. Ginzburg, and D.A. Kirzhnits, eds. (1982). High-Temperature Superconductivity (Consultance Bureau).
6. Hirschfeld, P.J., Korshunov, M.M., and Mazin, I.I. (2011). Gap symmetry and structure of Fe-based superconductors. Rep. Prog. Phys. *74*, 124508.
7. Li, B., Xing, Z.W., Huang, G.Q., and Liu, M. (2012). Magnetic-enhanced electron-phonon coupling and vacancy effect in "111"-type iron pnictides from first-principle calculations. J. Appl. Phys. *111*, 033922.
8. Coh, S., Cohen, M.L., and Louie, S.G. (2016). Antiferromagnetism enables electron-phonon coupling in iron-based superconductors. Phys. Rev. B *94*, 104505.
9. Deng, S., Köhler, J., and Simon, A. (2009). Electronic structure and lattice dynamics of NaFeAs. Phys. Rev. B *80*, 214508.
10. Coh, S., Cohen, M.L., and Louie, S.G. (2015). Large electron–phonon interactions from FeSe phonons in a monolayer. New J. Phys. *17*, 073027.
11. Masaki, S., Kotegawa, H., Hara, Y., Tou, H., Murata, K., Mizuguchi, Y., and Takano, Y. (2009). Precise Pressure Dependence of the Superconducting Transition Temperature of FeSe: Resistivity and 77Se-NMR Study. J. Phys. Soc. Jpn. *78*, 063704.
12. Peng, R., Shen, X.P., Xie, X., Xu, H.C., Tan, S.Y., Xia, M., Zhang, T., Cao, H.Y., Gong, X.G., Hu, J.P., et al. (2014). Measurement of an enhanced superconducting phase and a pronounced anisotropy of the energy gap of a strained FeSe single layer in FeSe/Nb:SrTiO3/KTaO3 heterostructures using photoemission spectroscopy. Phys. Rev. Lett. *112*, 107001.
13. Ge, J.F., Liu, Z.L., Liu, C., Gao, C.L., Qian, D., Xue, Q.K., Liu, Y., and Jia, J.F. (2015). Superconductivity above 100 K in single-layer FeSe films on doped $SrTiO_3$. Nat. Mater. *14*, 285–289.
14. Zhang, A.-M., and Zhang, Q.-M. (2013). Electron-phonon coupling in cuprate and iron-based superconductors revealed by Raman scattering. Chin. Phys. B *22*, 087103.
15. Wang, Z., Liu, C., Liu, Y., and Wang, J. (2017). High-temperature superconductivity in one-unit-cell FeSe films. J. Phys. Condens. Matter *29*, 153001.
16. Zhang, S., Guan, J., Wang, Y., Berlijn, T., Johnston, S., Jia, X., Liu, B., Zhu, Q., An, Q., Xue, S., et al. (2018). Lattice dynamics of ultrathin FeSe films on $SrTiO_3$. Phys. Rev. B *97*, 035408.
17. Jia, X.-W., Liu, H.-Y., Zhang, W.-T., Zhao, L., Meng, J.Q., Liu, G.-D., Dong, X.-L., Wu, G., Liu, R.-H., Chen, X.-H., et al. (2008). Common Features in Electronic Structure of the Oxypnictide Superconductor from Photoemission Spectroscopy. Chin. Phys. Lett. *25*, 3765–3768.
18. Zhang, C., Liu, Z., Chen, Z., Xie, Y., He, R., Tang, S., He, J., Li, W., Jia, T., Rebec, S.N., et al. (2017). Ubiquitous strong electron-phonon coupling at the interface of FeSe/$SrTiO_3$. Nat. Commun. *8*, 14468.
19. Stockert, U., Abdel-Hafiez, M., Evtushinsky, D.V., Zabolotnyy, V.B., Wolter, A.U.B., Wurmehl, S., Morozov, I., Klingeler, R., Borisenko, S.V., and Büchner, B. (2011). Specific heat and angle-resolved photoemission spectroscopy study of the superconducting gaps in LiFeAs. Phys. Rev. B *83*, 224512.
20. Miao, H., Qian, T., Shi, X., Richard, P., Kim, T.K., Hoesch, M., Xing, L.Y., Wang, X.C., Jin, C.Q., and Hu, J.P. (2015). Observation of strong electron pairing on bands without Fermi surfaces in $LiFe_{1-x}Co_xAs$. Nat. Commun. *6*, 6056.
21. Song, J., and Annett, J.F. (1995). Electron-phonon coupling and d-wave superconductivity in the cuprates. Phys. Rev. B *51*, 3840–3849.
22. Zhang, S.J., Wang, X.C., Sammynaiken, R., Tse, J.S., Yang, L.X., Li, Z., Liu, Q.Q., Desgreniers, S., Yao, Y., Liu, H.Z., and Jin, C.Q. (2009). Effect of pressure on the iron arsenide superconductor LixFeAs (x = 0.8, 1.0, 1.1). Phys. Rev. B *80*, 014506.
23. Wang, A.F., Xiang, Z.J., Ying, J.J., Yan, Y.J., Cheng, P., Ye, G.J., Luo, X.G., and Chen, X.H. (2012). Pressure effects on the superconducting properties of single-crystalline Co doped NaFeAs. New J. Phys. *14*, 113043.
24. Liu, D., Li, C., Huang, J., Lei, B., Wang, L., Wu, X., Shen, B., Gao, Q., Zhang, Y., Liu, X., et al. (2018). Orbital Origin of Extremely Anisotropic Superconducting Gap in Nematic Phase of FeSe Superconductor. Phys. Rev. X *8*, 031033.
25. Masaki, S., Kotegawa, H., Hara, Y., Tou, H., Murata, K., Mizuguchi, Y., and Takano, Y. (2009). Precise Pressure Dependence of the Superconducting Transition Temperature of FeSe: Resistivity and 77Se-NMR Study. J. Phys. Soc. Jpn. *78*, 063704.
26. Yamane, R., Komatsu, K., and Kagi, H. (2017). Note: Development of a new Bridgman-type high pressure cell for accurate dielectric measurements. Rev. Sci. Instrum. *88*, 046104.
27. Drozdov, A.P., Eremets, M.I., Troyan, I.A., Ksenofontov, V., and Shylin, S.I. (2015). Conventional superconductivity at 203 kelvin at high pressures in the sulfur hydride system. Nature *525*, 73–76.
28. Borisenko, S.V., Evtushinsky, D.V., Liu, Z.H., Morozov, I., Kappenberger, R., Wurmehl, S., Büchner, B., Yaresko, A.N., Kim, T.K., Hoesch, M., et al. (2016). Direct observation of spin–orbit coupling in iron-based superconductors. Nat. Phys. *12*, 311–317.

29. Wang, A.F., Xiang, Z.J., Ying, J.J., Yan, Y.J., Cheng, P., Ye, G.J., Luo, X.G., and Chen, X.H. (2012). Pressure effects on the superconducting properties of single-crystalline Co doped NaFeAs. New J. Phys. *14*, 113043.

30. Cong, L., Xianxin, W., Le, W., Defa, L., Yongqing, C., Yang, W., Qiang, G., Chunyao, S., Jianwei, H., Chenxiao, D., et al. (2020). Spectroscopic Evidence for an Additional Symmetry Breaking in the Nematic State of FeSe Superconductor. Phys. Rev. X *10*, 031033.

31. Qisi, W., Lara, F., and Anna, E.B. (2022). Editorial: Nematicity in iron-based superconductors. Front. Phys. *19*, 1038127. https://doi.org/10.3389/fphy.2022.1038127.

32. Weng, K.-C., and Hu, C.D. (2016). The p-wave superconductivity in the presence of Rashba interaction in 2DEG. Sci. Rep. *6*, 29919.

33. Kim, D.J. (1977). The influence of magnetism on the electron-phonon interaction in metals. Phys. B+C *91*, 281–287.

34. Wong, C.H., and Lortz, R. (2023). Preliminary T_c Calculations for Iron-Based Superconductivity in NaFeAs, LiFeAs, FeSe and Nanostructured FeSe/$SrTiO_3$ Superconductors. Materials *16*, 4674.

35. McMillian, W.L. (1968). Transition Temperature of Strong-Coupled Superconductors. Phys. Rev. *167*, 331.

36. König, E.J., and Coleman, P. (2019). Coulomb problem in iron-based superconductors. Phys. Rev. B *99*, 144522.

37. Liu, L., Xu, G., Wang, A., Wu, X., and Wang, R. (2017). First-principles investigations on structure stability, elastic properties, anisotropy and Debye temperature of tetragonal LiFeAs and NaFeAs under pressure. J. Phys. Chem. Solids *104*, 243–251.

38. Medvedev, S., McQueen, T.M., Troyan, I.A., Palasyuk, T., Eremets, M.I., Cava, R.J., Naghavi, S., Casper, F., Ksenofontov, V., Wortmann, G., et al. (2009). Electronic and magnetic phase diagram of β-$Fe_{1.01}Se$ with superconductivity at 36.7 K under pressure. Nat. Mater. *8*, 630–633.

39. Koufos, A.P., Papaconstantopoulos, D.A., and Mehl, M.J. (2014). First-principles study of the electronic structure of iron-selenium: Implications for electron-phonon superconductivity. Phys. Rev. B *89*, 035150.

STAR★METHODS

KEY RESOURCES TABLE

REAGENT or RESOURCE	SOURCE	IDENTIFIER
All analyzed data	This Study	

RESOURCE AVAILABILITY

Lead contact

Further information and requests for resources should be directed to the lead contact, Chi Ho Wong (chkhwong@ust.hk).

Materials availability

This study did not generate new unique reagents.

Data and code availability

- All data reported in this paper will be shared by the lead contact upon request.
- This paper does not report original code.
- Any additional information required to reanalyze the data reported in this paper is available from the lead contact upon request.

EXPERIMENTAL MODEL AND STUDY PARTICIPANT DETAILS

No experimental model and participant in this study.

METHOD DETAILS

Charge transfer in the tetrahedral regions in the presence of AFM-SDW

To avoid the high computational cost and time-consuming experimental effort involved in calibrating 'A' in the GGA+A functional for the emergence of the induced xy potential,[8,10] we propose a two-channel model for iron-based superconductors. In this model, we designate the upper tetrahedral plane as channel 1 and the lower tetrahedral plane as channel 2. By applying the superposition principle, we can independently calculate the induced xy potential arising from channel 1 and channel 2 individually. We define $R_{ph} \sim \frac{0.5(DOS_1^{XY}+DOS_2^{XY})}{DOS_{1\&2}^{XY}}$ where $DOS_{channel}^{XY}$ is the mean density of states of electrons within the ARPES range, where 'channel' can be '1' or '2', or '1&2'. We analyze the effect of the out-of-plane phonon vibration (+z and –z) on the electronic DOS, respectively. Specifically, the out-of-plane phonon vibration along the +z direction influences the DOS (so-called DOS_1^{XY}), while the out-of-plane phonon vibration along the -z direction affects the electronic DOS (so-called DOS_2^{XY}). To obtain an overall picture, we average the DOS values from both separate cases, resulting in <DOS> = (DOS_1^{XY} + DOS_2^{XY})/2. Due to symmetry considerations, $DOS_1^{XY} = DOS_2^{XY}$ (unless otherwise specified). On the other hand, the redistribution of AFM fluctuations under SDW leads to a much stronger local AFM fluctuation alternatingly, where R_{SDW} is always 2 based on the conservation of antiferromagnetic energy.

ARPES analysis

This factor accounts for the average electron-phonon scattering matrix within the spectral weight shift range of ARPES data[17–19] The dielectric constant, denoted by ε, regulates the screening effect when there is interaction among all relevant electrons associated with the induced xy potential. By incorporating the ARPES factor, the electron-phonon scattering matrix g increases by $R_{ARPES} \sim \frac{\langle \sum_{E_F-E_{Debye}}^{E_F} g_{pp'}(E')/\varepsilon' \rangle}{g_{pp'}(E_F)/\varepsilon}$.

Anisotropic k space

Concerning the momentum dependence of the superconducting gap, we use the anisotropic wavevector in the literature.[20,24] The anisotropic momentum space is modeled by an ellipse equation approximately, $p_{angular}(\theta) = \frac{a_{major}b_{minor}}{\sqrt{(b_{minor}{}^2 - a_{major}{}^2)\cos^2\theta + a_{major}{}^2}}$. The major *a* and minor *b* axes determine the extent $f_{anisotropy}$ to which the relative area of anisotropic momentum space ($\int \frac{1}{2} p_{angular}(\theta)^2 d\theta$), deviates from a perfect circle. To monitor the 4-fold superconducting gap, it may be necessary to observe the overlapping of two ellipses (please see Figure 1A).

AFM & SDW amplified electron-phonon interaction under spin-orbital coupling

The spin-orbital coupling (SOC) of IBSC is commonly around 10meV.[28] It is reasonable to consider the influence of SOC to electron-phonon interaction. In the presence of the Coh factor[8] ($R_{SDW} \cdot R_{ph}$) and ARPES factor, the ionic potential becomes $V_{XY} R_{ph}$ and the Eliashberg function may be written as

$$\alpha^2 F(\omega) \sim \left\langle \sum_{V_{E_F} - V_{Debye}}^{V_{E_F}} \int \frac{d^2 p_E}{v_E} \right\rangle \left\langle \sum_{V_F - V_{Debye}}^{V_F} \int \frac{d^2 p_E{}'}{(2\pi\hbar)^3 v_E{}'} \right\rangle$$
$$\sum_{v} \delta(\omega - \omega_{p-p'v}) \left| \sqrt{\frac{\hbar}{C\omega_{p-p'v}}} \int u_i \cdot \nabla (V_{XY} R_{ph}) \psi_p^* R_{SDW} R_{ARPES} \psi_{p'} dr \right|^2 \Big/ \left\langle \sum_{V_{E_F} - V_{Debye}}^{V_{E_F}} \int \frac{d^2 p_E}{v_E} \right\rangle$$

where $\langle \sum_{V_F - V_{Debye}}^{V_F} \int \frac{d^2 p_E}{v_E} \rangle$ is the surface integral at different electron energies within the ARPES range and $v_E \in (v_{E_F} - v_{Debye}, v_{E_F})$. The velocity v_{Debye} is converted from the Debye energy and $F(\omega)$ is phonon data. The Planck constant is $\hbar$ and C is a material constant. The pairing strength become $\lambda \sim 2 \int \alpha^2 \frac{F(\omega)}{\omega} d\omega$[35] where $\alpha^2 \sim \alpha^2_{E_F}(f_{anisotropy}) R^2_{AFM} R^2_{Ph} R^2_{SDW} R^2_{ARPES}$. R^2_{AFM} is always above 1 when electron-phonon calculation is switched from spin-restricted to spin-unrestricted situation. When strong coupling is observed, the renormalized electron-phonon coupling and pseudopotential are expressed as $\lambda^*_{PS} = \frac{\lambda_{PS}}{\lambda_{PS}+1}$ and $\mu^* = \frac{\mu}{\lambda_{PS}+1}$, respectively.[35] $f_{anisotropy}$ equals to 1 for an isotropic momentum space. The variation of the exchange interaction, $f(E_{ex}) \sim \frac{[M_{Fe} M_{Fe} E_{co}]_{P>0}}{[M_{Fe} M_{Fe} E_{co}]_{P=0}}$ under applied pressure P, can be monitored using the pressure dependence of the antiferromagnetic interaction. The value of $f(E_{ex})$ is controlled by magnetic moment of Fe atom M_{Fe} and exchange correlation energy E_{co}.

In the context of energy transfer from AFM fluctuations to electron-phonon coupling, it is observed that the maximum AFM interactions between two neighboring Fe atoms can only double their own AFM energy in a repeating unit. However, it leads to a result that the electron-phonon interaction is amplified by a factor of $2^2 = 4$, thereby suggesting the presence of higher-order AFM fluctuations. We will compare the calculated T_c values for 1st order and 2nd order AFM fluctuations as a function of pressure. If the compressed sample is under the 1st order AFM fluctuation, we set $R^2_{Ph}|_{P>0} \sim R^2_{Ph}|_{P=0} \cdot f(E_{ex})$ and $R^2_{AFM}|_{P>0} \sim R^2_{AFM}|_{P=0} \cdot f(E_{ex})$. Otherwise, we set $R^2_{Ph}|_{P>0} \sim R^2_{Ph}|_{P=0} \cdot f(E_{ex})^2$ and $R^2_{AFM}|_{P>0} \sim R^2_{AFM}|_{P=0} \cdot f(E_{ex})^2$. Although the accuracy of calculating the pseudopotential for a strongly correlated electron system, such as Fe-based superconductors, as a function of Debye temperature and Fermi level,[36] may not be very precise, it has been suggested that the value should be approximately 0.15 for most Fe-based superconductors.[36] We put the ab-initio details in the supplemental information.

QUANTIFICATION AND STATISTICAL ANALYSIS

The T_c resulting from first vs. second-order antiferromagnetic fluctuations is pivotal for achieving success in this formula. The data is computed in CASTEP where the accuracy is high enough to ensure that the data is not functionally/parametrically dependent. This is not a statistical model and hence no statistical analysis is reported here.